1. NLO EW technical and physics comparisons[1, 2]

Adequate predictions for scattering processes at particle colliders such as the LHC require the inclusion of next-to-leading order (NLO) perturbative corrections of the strong and electroweak (EW) interactions. For the calculation of NLO QCD corrections the automation has been established, and several tools exist [1, 2, 3, 4, 5, 6, 7, 8, 9]. On the other hand, the automation of NLO EW corrections has just started, and only a few tools are available [10, 11, 12, 13]. In this section we review the status of the existing tools for the automated calculation of EW one-loop amplitudes and provide a comparison of some of them for specific processes. In addition, we also show a comparison of the Sudakov approximation for the EW corrections as implemented in ALPGEN [14] with complete NLO calculations. Finally, we present a comparison of theoretical predictions from various codes with experimental results from CMS for the ratio of the associated production of a Z/γ^* or an on-shell photon with additional jets as a function of the transverse momentum of the vector boson.

1.1 Codes for the automated calculation of electroweak NLO corrections

RECOLA

RECOLA is a Fortran95 computer program for the automated generation and numerical computation of scattering amplitudes in the full Standard Model (SM) (including QCD and the EW sector) at tree and one-loop level. It is based on a one-loop generalization of Dyson–Schwinger recursion relations [15] and allows to generate one-loop amplitudes for (in principle) arbitrary decay and scattering processes in the SM with particular emphasis on high particle multiplicities. Counterterms [16] and rational terms [17] are included via dedicated tree-level Feynman rules. RECOLA was the first automated tool to calculate EW NLO corrections [10].

RECOLA provides numerical results for scattering amplitudes in the 't Hooft–Feynman gauge. Dimensional regularization is used for ultraviolet singularities, while collinear and soft singularities can be treated either in dimensional or in mass regularization. RECOLA is interfaced to the COLLIER library [18, 19] for the fast and numerically stable calculation of one-loop tensor integrals. For renormalization, apart from the traditional on-shell scheme [16], RECOLA in particular features its generalization to the complex-mass scheme [20]. RECOLA further supports the G_μ, the $\alpha(0)$ and the $\alpha(M_\mathrm{Z})$ scheme for the renormalization of the electromagnetic coupling constant, and a dynamical N_f-flavour scheme for the strong coupling constant. Internal resonant particles can be treated in the complex-mass scheme. Moreover, resonant contributions can be consistently isolated such that matrix elements involving specific intermediate resonances can be calculated. The calculation of squared amplitudes, summed over spin and colour, is supported at leading order (LO), NLO, and for loop-induced processes. Besides the calculation of complete tree-level and one-loop results, RECOLA allows to select or discard specific orders of α_s (and thus also of α) in all computed objects, such as in the amplitudes, in the square of the Born amplitude or in the interference of the Born with the one-loop amplitude. Moreover, the code allows the computation of colour- and spin-correlated LO squared amplitudes required for dipole subtraction [21, 22].

For the calculation of physical cross sections RECOLA has to be interfaced to a Monte Carlo code or a multi-purpose event generator; such interfaces are presently being developed. Together with private Monte Carlo integrators, RECOLA has been used for the computation of EW corrections to $\mathrm{pp} \to \mathrm{l^+l^-jj}, \nu_\mathrm{l}\bar{\nu}_\mathrm{l}\mathrm{jj}$ [23] and the QCD corrections to $\mathrm{pp} \to \mathrm{e^+}\nu_\mathrm{e}\mu^-\bar{\nu}_\mu\mathrm{b\bar{b}H}$ [24].

[1] Section coordinators: V. Ciulli, A. Denner

[2] Contributing authors: M. Chiesa, R. Frederix, L. Hofer, S. Kallweit, J.M. Lindert, P. Maierhöfer, A. Marini, G. Montagna, M. Moretti, O. Nicrosini, D. Pagani, F. Piccinini, S. Pozzorini, M. Schönherr, E. Takasugi, S. Uccirati, M.A. Weber, M. Zaro

SHERPA/MUNICH+OPENLOOPS

The frameworks MUNICH + OPENLOOPS and SHERPA + OPENLOOPS automate the full chain of operations – from process definition to collider observables – that enter NLO QCD+EW simulations at parton level. The relevant scattering amplitudes at NLO QCD are publicly available in the form of an automatically generated library [25] that supports all interesting LHC processes (more than one hundred processes), can be easily extended upon user request and will be extended to NLO EW soon. The recently achieved automation of EW corrections [11, 26] is based on the well established QCD implementations and allows for NLO QCD+EW simulations for a vast range of SM processes, up to high particle multiplicity, at current and future colliders. To be precise, the new implementations allow for NLO calculations at any given order $\alpha_s^n\alpha^m$, including all relevant QCD–EW interference effects. Full NLO SM calculations that include all possible $\mathcal{O}(\alpha_s^{n+k}\alpha^{m-k})$ contributions to a certain process are also supported.

In these frameworks virtual amplitudes are provided by the OPENLOOPS program [25], which is based on the Open Loops algorithm [9] – a fast numerical recursion for the evaluation of one-loop scattering amplitudes. The extension to NLO EW corrections required the implementation of all $\mathcal{O}(\alpha)$ EW Feynman rules in the framework of the numerical Open Loops recursion including counterterms associated with so-called R_2 rational parts [17] and with the on-shell renormalization of UV singularities [16]. Additionally, for the treatment of heavy unstable particles the complex-mass scheme [20] has been implemented in a fully general way. Combined with the COLLIER tensor-reduction library [18], which implements the Denner–Dittmaier reduction techniques [27, 28] and the scalar integrals of Ref. [29], or with CUTTOOLS [30], which implements the OPP method [31], together with the ONELOOP library [32], the employed recursion permits to achieve very high CPU performance and a high degree of numerical stability.

All remaining tasks, i.e. the bookkeeping of partonic subprocesses, phase-space integration and the subtraction of QCD and QED bremsstrahlung are supported by the two independent and fully automated Monte Carlo generators MUNICH [33] and SHERPA [34, 35]. The first one, MUNICH, is a fully generic and very fast parton-level Monte Carlo integrator. SHERPA is a particle-level Monte Carlo generator providing all stages of hadron-collider simulations, including parton showering, NLO matching, multi-jet merging, hadronization and underlying event simulations. For tree amplitudes, with all relevant colour and helicity correlations, MUNICH relies on OPENLOOPS, while SHERPA generates them internally with AMEGIC++ [36] and COMIX [37]. For the cancellation of infrared singularities both Monte Carlo tools, MUNICH and SHERPA, employ the dipole-subtraction scheme [21, 22] and its extension to EW corrections [38, 39]. Both codes were extensively checked against each other, and sub-permille level agreement was found. The implementation of parton-shower matching and multi-jet merging including NLO EW effects is available in an approximate way [26], while a fully consistent implementation is under way.

Employing the described frameworks in Ref. [11] the simulation of $\mathrm{W} + 1, 2, 3$ jet production at NLO EW+QCD was presented. In order to make the calculation of the process with the highest jet multiplicity feasible, it was important to factorize these processes into a production part and into a decay part. At the NLO EW level this required a careful implementation of the narrow-width approximation in order to control numerical stability given the appearance of pseudo-resonances for two or more associated jets. It was found that V + multijet final states feature genuinely different EW effects as compared to the case of $V + 1$ jet. Subsequently in Ref. [26] NLO QCD+EW simulations were presented for $\mathrm{Z} +$ jets and $\mathrm{W}^{\pm} +$ jets production including off-shell leptonic decays and multijet merging with up to two jets within the MEPS@NLO framework of the SHERPA Monte Carlo program.

MADGRAPH5_AMC@NLO

The results presented in Section 1.2 have been obtained via an extension of the public code MADGRAPH5_AMC@NLO [40] that allows to automatically calculate also NLO EW corrections. This version

of the code is, at the moment, private and has already been used for the calculation of NLO QCD and EW corrections to the hadroproduction of a top-quark pair in association with a heavy boson [12, 41].

The automation of the NLO QCD and EW corrections for a generic SM process has required major improvements for all the building blocks of the MADGRAPH5_AMC@NLO code [42, 6]. The generation of the amplitudes and matrix elements at LO and NLO accuracy for the combined expansion in powers of α_s and α has been lengthly discussed in Refs. [40, 12]. The code at the moment is able to automatically calculate all the possible perturbative orders stemming from tree-level amplitudes and their interference with one-loop amplitudes, for any SM process. Moreover, it is possible to select any combination of perturbative orders. Thus, all the necessary R_2 and UV counterterms have been calculated both in the complex-mass scheme and with real masses and on-shell renormalization conditions for unstable particles. These counterterms are part of the so-called NLO UFO models [43], which is the general format used in MADGRAPH5_AMC@NLO for importing Feynman rules of a given Lagrangian. In the case of the SM at NLO, two different UFO models have been created in order to calculate EW corrections respectively in the $\alpha(m_{\rm Z})$ or G_μ scheme.

The subtraction of infrared divergences and the integration over the Born-like and real-emission phase space is automatically performed for any process by extending the framework described in Refs. [40, 42], taking into account all the EW-QCD IR divergences appearing at any perturbative order that enter into NLO predictions.

At the moment, NLO corrections for massive-only final states can be automatically calculated by running a code that can be generated in MADGRAPH5_AMC@NLO via few commands of the form:[3]

```
import model QCDandEW_renormalization-scheme
generate process QCD=m QED=n [QCD QED]
output process_at_orders_m_n_with_QCD_and_QED_corrections
```

The indices m and n and the flags QCD and QED can be used to select the desired perturbative orders. In the case of massless final states, code-wise no additional improvement is required. However, with QCD and EW corrections a generic approach for the treatment of IR divergences and a IR-safe definition of final-state products is not straightforward. Thus, besides the generation of the code on the same line of the case of massive-only final states, with massless particle specific solutions are necessary to obtain IR-safe definition of the final state, as done, e.g. in Refs. [11, 23], which are considered in these proceedings.

At the moment results can be obtained only at fixed order, without matching to shower effects. The matching with QED or in general EW shower will be also included in the future, by extending the matching procedure with QCD parton showers that is already available in the public version of the code.

1.2 Technical comparison of EW NLO cross sections

In order to assess the status of the automated tools for the calculation of EW corrections a technical comparison has been performed. Given the complexity of this enterprise, we have chosen the recent calculations of EW corrections to $\rm pp \to l^+l^- + 2\,jets$, $\rm pp \to l^+\nu + 2\,jets$, and $\rm pp \to t\bar{t}H$ obtained with the automated tools RECOLA, SHERPA/MUNICH+OPENLOOPS, and MADGRAPH5_AMC@NLO, respectively and published in Refs. [23, 26, 41]. We invited all other groups to provide numbers for comparison with specific results in these publications and in addition some cumulative histograms using the setups of the respective publications. While the SHERPA/MUNICH+OPENLOOPS collaboration provided numbers for all three processes, none of the other groups delivered new results for comparison.

The input parameters and set-ups of the calculations in Refs. [23, 26, 41] are summarized in Table 1. The large number of parameters and settings that have to be adapted reflects the complexity of the calculations. Note that $\hat{H}_{\rm T}$ is calculated from the sum of transverse energies of all final-state

[3] These are representative commands, the future public version of the code may have to be used with different syntax.

particles, i.e.

$$\hat{H}_{\mathrm{T}} = \sum_i E_{\mathrm{T,i}} = \sum_i \sqrt{p_{\mathrm{T,i}}^2 + m_i^2}, \tag{1}$$

while H_{T} from the sum of all transverse momenta,

$$H_{\mathrm{T}} = \sum_i p_{\mathrm{T,i}}. \tag{2}$$

The calculation of the factorization and renormalization scale for $\mathrm{pp} \to \mathrm{l}^+\nu + 2\,\text{jets}$, is performed using the transverse energy of the lepton–neutrino system,

$$\hat{H}'_{\mathrm{T}} = p_{\mathrm{T,j_1}} + p_{\mathrm{T,j_2}} + p_{\mathrm{T,g}} + p_{\mathrm{T},\gamma} + E_{\mathrm{T,l}\nu}, \qquad E_{\mathrm{T,l}\nu} = \sqrt{p_{\mathrm{T,l}\nu}^2 + m_{\mathrm{l}\nu}^2}. \tag{3}$$

Radiated partons and photons are included at NLO. The cuts for the processes $\mathrm{pp} \to \mathrm{l}^+\mathrm{l}^- + 2\,\text{jets}$ and $\mathrm{pp} \to \mathrm{l}^+\nu + 2\,\text{jets}$ are listed in Table 2, while no cuts have been applied for $\mathrm{pp} \to \mathrm{t\bar{t}H}$. The jet with highest transverse momentum is denoted $\mathrm{j_1}$ in the following.

In Table 3 we present a comparison of results from RECOLA and SHERPA/MUNICH+OPENLOOPS for the process $\mathrm{pp} \to \mathrm{l}^+\mathrm{l}^- + 2\,\text{jets}$ in the setup defined in Tables 1 and 2. The results for the LO cross sections σ^{LO} including all SM tree-level contributions of order $\mathcal{O}(\alpha_s^2\alpha^2)$, $\mathcal{O}(\alpha_s\alpha^3)$, and $\mathcal{O}(\alpha^4)$, agree within 0.5% or better. The relative EW corrections $\delta_{\mathrm{EW}}^{\mathrm{NLO}} = \delta\sigma_{\mathrm{EW}}^{\mathrm{NLO}}/\sigma^{\mathrm{LO}}$, where $\delta\sigma_{\mathrm{EW}}^{\mathrm{NLO}}$ contains the complete NLO corrections of order $\mathcal{O}(\alpha_s^2\alpha^3)$, agree at the level of $\mathcal{O}(1\%)$ or better. The difference in the NLO EW correction factors can be attributed to a different treatment of b-quark-initiated processes and of final-state photon radiation. While both calculations use democratic clustering for jets and photons, in Ref. [23] the quark–photon fragmentation function has been used for a consistent photon–jet separation; in the SHERPA/MUNICH+OPENLOOPS approach the cancellation of collinear singularities is enforced by recombining (anti)quark-photon pairs in a tiny cone around the singular region as described in Ref. [11]. While in the calculation of Ref. [23] the contributions of bottom quarks have been neglected at NLO, these are included in the calculation based on SHERPA/MUNICH+OPENLOOPS. Note that the agreement for $\delta_{\mathrm{EW}}^{\mathrm{NLO}}$ is better for large transverse momenta, where the contributions of b-quark-initiated processes are small.

In Table 4 we present results from SHERPA/MUNICH+OPENLOOPS for the process $\mathrm{pp} \to \mathrm{l}^+\nu + 2\,\text{jets}$ in the setup defined in Tables 1 and 2. The results for the LO cross sections $\sigma_{\mathrm{QCD}}^{\mathrm{LO}}$ include the tree-level contributions of order $\mathcal{O}(\alpha_s^2\alpha^2)$; the relative QCD corrections, $\delta_{\mathrm{QCD}}^{\mathrm{NLO}} = \delta\sigma_{\mathrm{QCD}}^{\mathrm{NLO}}/\sigma_{\mathrm{QCD}}^{\mathrm{LO}}$, and EW corrections, $\delta_{\mathrm{EW}}^{\mathrm{NLO}} = \delta\sigma_{\mathrm{EW}}^{\mathrm{NLO}}/\sigma_{\mathrm{QCD}}^{\mathrm{LO}}$, involve the complete NLO contributions of order $\mathcal{O}(\alpha_s^3\alpha^2)$ and $\mathcal{O}(\alpha_s^2\alpha^3)$, respectively. While none of the other groups provided results for this process, we nevertheless show these numbers as benchmarks for future comparisons. Moreover, in Section 1.3 these results are compared with a calculation in the Sudakov approximation for the EW corrections.

In Table 5 we present a comparison of results from MADGRAPH5_AMC@NLO and SHERPA/MUNICH+OPENLOOPS for the process $\mathrm{pp} \to \mathrm{t\bar{t}H}$ in the inclusive setup defined in Table 1. The relative corrections are normalized to the LO QCD cross section, $\delta_X^{\mathrm{NLO}} = \delta\sigma_X^{\mathrm{NLO}}/\sigma_{\mathrm{QCD}}^{\mathrm{LO}}$. The absolute QCD corrections, $\delta\sigma_{\mathrm{QCD}}^{\mathrm{NLO}}$ and EW corrections $\delta\sigma_{\mathrm{EW}}^{\mathrm{NLO}}$ comprise the complete NLO contributions of order $\mathcal{O}(\alpha_s^3\alpha)$ and $\mathcal{O}(\alpha_s^2\alpha^2)$, respectively. For the entries with "no γ" the PDF of the photon has been artificially set to zero in order to gauge the impact of photons in the initial state. All the results are at per mille accuracy w.r.t. the corresponding LO QCD predictions. In the SHERPA/MUNICH+OPENLOOPS calculation, a six-flavour scheme is employed, consistently with the NNPDF2.3_QED PDF distribution. The gluon splitting into top-quark pairs in the PDF evolution as well as the six-flavour running and renormalization of α_s are taken into account. However, contributions from initial-state top quarks and top-quark bremsstrahlung are not included. This is justified by the fact that the former are formally of order $\alpha_s^2 \log^2(\mu_{\mathrm{R}}/m_{\mathrm{t}})$, while top-bremsstrahlung gives rise to Higgs+multi-top signatures. Conversely,

parameter/setting	$pp \to l^+l^- + 2\,\text{jets}$	$pp \to l^+\nu + 2\,\text{jets}$	$pp \to t\bar{t}H$
order of LO contribution	all	$\mathcal{O}(\alpha_s^2\alpha^2)$	$\mathcal{O}(\alpha_s^2\alpha)$
order of NLO corrections	$\mathcal{O}(\alpha_s^2\alpha^3)$	$\mathcal{O}(\alpha_s^3\alpha^2), \mathcal{O}(\alpha_s^2\alpha^3)$	$\mathcal{O}(\alpha_s^3\alpha), \mathcal{O}(\alpha_s^2\alpha^2)$
renormalization scheme	G_μ scheme	G_μ scheme	$\alpha(M_\text{Z})$ scheme
complex/real masses	complex-mass scheme	complex-mass scheme	real masses
jet algorithm	anti-k_T, $R = 0.4$	anti-k_T, $R = 0.4$	–
partons clustered for	$\lvert y\rvert < 5$	$\lvert y\rvert < \infty$	–
photon/jet separation	democratic clustering + fragmentation	fermion–photon recombination and democratic clustering	–
$\max \frac{E_\gamma}{E_\gamma + E_j}$	0.7	0.5	–
PDF set	MSTW2008LO	NNPDF2.3QED	NNPDF2.3QED
factorization scale	$M_{\text{Z,pole}}$	$\hat{H}'_\text{T}/2$	$\hat{H}_\text{T}/2$
renormalization scale	$M_{\text{Z,pole}}$	$\hat{H}'_\text{T}/2$	$\hat{H}_\text{T}/2$
partons at LO	g,u,c,d,s,b	g,u,c,d,s,b	g,u,c,d,s,b,γ
partons at NLO	g,u,c,d,s	g,u,c,d,s,b	g,u,c,d,s,b,γ
γ-induced contributions	none	only at LO	all/none
collider energy	13 TeV	13 TeV	13 TeV
α_s (from PDF)	$0.139395\ldots$	0.118	0.118
G_μ [GeV^{-2}]	$1.1663787 \cdot 10^{-5}$	$1.16637 \cdot 10^{-5}$	calculated from α
α	calculated from G_μ	calculated from G_μ	$1/128.93$
$M_{\text{Z,on-shell}}$	91.1876 GeV	91.1876 GeV	91.188 GeV
$\Gamma_{\text{Z,on-shell}}$	2.4952 GeV	2.4955 GeV	0 GeV
$M_{\text{Z,pole}}$, $\Gamma_{\text{Z,pole}}$	calculated	–	–
$M_{\text{W,on-shell}}$	80.385 GeV	80.385 GeV	80.385 GeV
$\Gamma_{\text{W,on-shell}}$	2.085 GeV	2.0897 GeV	0 GeV
$M_{\text{W,pole}}$, $\Gamma_{\text{W,pole}}$	calculated	–	–
complex masses	from pole masses	from on-shell masses	–
m_b	0 GeV	0 GeV	0 GeV
m_t	173.2 GeV	173.2 GeV	173.3 GeV
Γ_t	0 GeV	1.339 GeV	0 GeV
M_H	125 GeV	125 GeV	125 GeV
Γ_H	0 GeV	4.07 MeV	0 GeV

Table 1: Settings and input parameters used for technical comparisons.

$pp \to l^+l^- + 2\,\text{jets}$	$pp \to l^+\nu + 2\,\text{jets}$
$p_{T,j} > 30$ GeV	$p_{T,j} > 30$ GeV
$\lvert y_j \rvert < 4.5$	$\lvert \eta_j \rvert < 4.5$
$p_{T,l} > 20$ GeV	$p_{T,l} > 25$ GeV
$\lvert y_l \rvert < 2.5$	$\lvert \eta_l \rvert < 2.5$
$\Delta R_{ll} > 0.2$	$\Delta R_{jl} > 0.5$
$\Delta R_{jl} > 0.5$	$M_{T,W} > 40$ GeV
66 GeV $< M_{ll} < 116$ GeV	$E_{T,miss} > 25$ GeV

Table 2: Cuts used for technical comparisons.

the results from MADGRAPH5_AMC@NLO are obtained within the five-flavour scheme, renormalizing top-quark loops in the decoupling scheme. This means that top-quark contributions to the initial state and to the Bremsstrahlung should not be included in the hard cross section, and a running α_s with five active flavours should be employed. Therefore, one has to compensate the inputs from the NNPDF2.3_QED PDF distribution, i.e. the luminosities and α_s for given Bjorken x's and scales, which are in the six-flavour scheme, to be consistent with the five-flavour scheme approach used in the matrix elements.[4] In practice, both approaches are internally consistent, and the different treatments of the α_s evolution are exactly equivalent, as $\log(\mu_R/m_t)$ terms turn out to be accounted for to all orders in both calculations. However, the fact that top-quark contributions to the evolution of the gluon density are taken into account (through the NNPDF2.3_QED PDFs) in SHERPA/MUNICH+OPENLOOPS and are subtracted in MADGRAPH5_AMC@NLO gives rise to a difference of $\mathcal{O}(\alpha_s \log(\mu_F/m_t))$, which manifests itself as one-percent level deviations in the numerical predictions.

1.3 Comparison of Sudakov approximation with EW NLO corrections for distributions

In Refs. [45, 46] a process-independent algorithm for the computation of one-loop EW corrections has been developed. According to the algorithm, the $\mathcal{O}(\alpha)$ corrections to a generic process involving N external particles of flavour $i_1, \cdots, i_N$ factorize in the high-energy limit as follows:

$$\delta\mathcal{M}^{\text{NLL}}_{i_1\cdots i_n}\Big|_{\text{Sudakov}} = \sum_{k=1}^{N}\sum_{l>k}\delta^{\text{DL}}_{kl}\mathcal{M}^{\text{LO}}_{i_1\cdots j_k\cdots j_l\cdots i_n} + \sum_{k=1}^{N}\delta^{\text{SL}}_{k}\mathcal{M}^{\text{LO}}_{i_1\cdots j_k\cdots i_n} + \delta^{\text{PR}}\mathcal{M}^{\text{NLL}}_{i_1\cdots i_n}. \tag{4}$$

In Eq. (4), the functions δ^{DL}_{kl} and δ^{SL}_{k} contain the Sudakov double and single logarithmic contributions, respectively. They depend only on the flavour and on the kinematics of the external particles. These terms multiply LO matrix elements that are obtained from the one of the original process $\mathcal{M}^{\text{LO}}_{i_1\cdots i_n}$ via $\text{SU}(2)$ transformations of pairs or single external legs, j_k being in Eq. (4) the $\text{SU}(2)$ transformed of the

[4] While NNPDF2.3_QED PDF distributions are in the variable-flavour scheme, with our choice of the scale, which is always larger than m_t, the variable-flavour scheme is equivalent to the six-flavour scheme. In order to remove the impact of the sixth flavour, one has to compensate its contribution to the running of α_s and to the DGLAP equation for the PDF evolution. At NLO QCD, this corresponds to

$$\sigma^{\text{NLO}}_{\text{QCD (6f-PDFs)}} = \sigma^{\text{NLO}}_{\text{QCD}} + \alpha_s\frac{2T_F}{3\pi}\left[\log\left(\frac{m_t^2}{\mu_R^2}\right)\sigma^{\text{LO}}_{\text{QCD,q}\bar{\text{q}}} + \log\left(\frac{\mu_F^2}{\mu_R^2}\right)\sigma^{\text{LO}}_{\text{QCD,gg}}\right]$$

as explained in Ref. [44], where the same issue has been addressed for the five- and the four-flavour scheme. The quantities $\sigma^{\text{LO}}_{\text{QCD,q}\bar{\text{q}}}$ and $\sigma^{\text{LO}}_{\text{QCD,gg}}$ correspond to the LO QCD cross sections from respectively only the $q\bar{q}$ and gg initial states. By setting $\mu_F = \mu_R$, as done here, the term proportional to $\sigma^{\text{LO}}_{\text{QCD,gg}}$ in the r.h.s. of Eq. (4) is equal to zero. In Ref. [41] the $N_f = 5$ scheme was used in combination with NNPDF2.3_QED without including such a subtraction term.

$pp \to l^+l^- + 2\,j$		RECOLA		SHERPA/MUNICH+OPENLOOPS	
G_μ scheme		[arXiv:1411.0916]			
		σ^{LO} [fb]	δ^{NLO}_{EW} [%]	σ^{LO} [fb]	δ^{NLO}_{EW} [%]
$p_{T,j_1} >$	0.0 TeV	$5.120 \cdot 10^4$	-2.5	$5.122 \cdot 10^4$	-3.4
	0.25 TeV	$2.071 \cdot 10^3$	-7.6	$2.072 \cdot 10^3$	-8.5
	0.5 TeV	$2.060 \cdot 10^2$	-13.1	$2.061 \cdot 10^2$	-13.7
	0.75 TeV	$3.603 \cdot 10^1$	-17.5	$3.603 \cdot 10^1$	-17.4
	1.0 TeV	$7.806 \cdot 10^0$	-21.5	$7.801 \cdot 10^0$	-20.5
$M_{j_1 j_2} >$	0.5 TeV	$4.203 \cdot 10^3$	-4.3	$4.202 \cdot 10^4$	-5.1
	1.0 TeV	$8.085 \cdot 10^2$	-5.8	$8.088 \cdot 10^2$	-6.5
	2.0 TeV	$8.377 \cdot 10^1$	-7.3	$8.368 \cdot 10^1$	-7.9
	4.0 TeV	$2.485 \cdot 10^0$	-8.2	$2.476 \cdot 10^0$	-8.4
$p_{T,\ell^-} >$	0.25 TeV	$3.176 \cdot 10^2$	-12.9	$3.177 \cdot 10^2$	-14.4
	0.5 TeV	$2.099 \cdot 10^1$	-20.5	$2.097 \cdot 10^1$	-20.3
	0.75 TeV	$2.673 \cdot 10^0$	-26.3	$2.676 \cdot 10^0$	-27.3
	1 TeV	$4.552 \cdot 10^{-1}$	-30.9	$4.532 \cdot 10^{-1}$	-31.3
$p_{T,\ell\ell} >$	0.25 TeV	$1.356 \cdot 10^3$	-9.3	$1.356 \cdot 10^3$	-10.9
	0.5 TeV	$1.094 \cdot 10^2$	-16.4	$1.093 \cdot 10^2$	-17.5
	0.75 TeV	$1.528 \cdot 10^1$	-22.0	$1.526 \cdot 10^1$	-21.1
	1.0 TeV	$1.879 \cdot 10^0$	-27.1	$1.873 \cdot 10^0$	-27.7
$H_T >$	0.5 TeV	$3.293 \cdot 10^3$	-7.1	$3.294 \cdot 10^3$	-8.0
	1.0 TeV	$3.012 \cdot 10^2$	-12.8	$3.012 \cdot 10^2$	-13.2
	1.5 TeV	$5.166 \cdot 10^1$	-17.6	$5.165 \cdot 10^1$	-16.8
	2.0 TeV	$1.087 \cdot 10^1$	-21.8	$1.087 \cdot 10^1$	-19.0

Table 3: Comparison of results from SHERPA/MUNICH+OPENLOOPS for $pp \to l^+l^- + 2\,\text{jets}$ in the setup defined in Tables 1 and 2.

$pp \to l^+\nu + 2j$		SHERPA/MUNICH+OPENLOOPS		
G_μ scheme		[arXiv:1511.08692]		
		σ^{LO}_{QCD}	δ^{NLO}_{QCD}	δ^{NLO}_{EW}
		[pb]	[%]	[%]
$p_{T,j_1} >$	0 TeV	$1.114 \cdot 10^{2}$	15.2	−2.7
	0.5 TeV	$1.551 \cdot 10^{-1}$	2.3	−12.5
	1 TeV	$4.092 \cdot 10^{-3}$	8.7	−19.5
$E_{T,miss} >$	0.5 TeV	$7.863 \cdot 10^{-3}$	−4.6	−22.4
	1 TeV	$7.863 \cdot 10^{-3}$	−2.9	−27.9
$p_{T,l^+} >$	0.5 TeV	$1.647 \cdot 10^{-2}$	0.1	−21.1
	1 TeV	$2.912 \cdot 10^{-4}$	0.6	−30.4
$H_T >$	0.5 TeV	$1.2635 \cdot 10^{0}$	12.3	−8.0
	1 TeV	$2.304 \cdot 10^{-1}$	58.6	−12.3
	2 TeV	$5.749 \cdot 10^{-3}$	61.9	−18.0

Table 4: Results from SHERPA/MUNICH+OPENLOOPS for $pp \to l^+\nu + 2$ jets in the setup defined in Tables 1 and 2.

$pp \to t\bar{t}H$	MADGRAPH5_AMC@NLO				SHERPA/MUNICH+OPENLOOPS			
$\alpha(M_Z)$ scheme	[arXiv:1504.03446]							
	σ^{LO}_{QCD}	δ^{NLO}_{QCD}	δ^{NLO}_{EW}	$\delta^{NLO}_{EW,\text{ no }\gamma}$	σ^{LO}_{QCD}	δ^{NLO}_{QCD}	δ^{NLO}_{EW}	$\delta^{NLO}_{EW,\text{ no }\gamma}$
	[pb]	[%]	[%]	[%]	[pb]	[%]	[%]	[%]
incl.	$3.617 \cdot 10^{-1}$	28.9	−1.2	−1.4	$3.617 \cdot 10^{-1}$	28.3	−1.3	−1.4
$p_{T,H/t/\bar{t}} > 200$ GeV	$1.338 \cdot 10^{-2}$	23.4	−8.2	−8.5	$1.338 \cdot 10^{-2}$	22.5	−8.2	−8.4
$p_{T,H/t/\bar{t}} > 400$ GeV	$3.977 \cdot 10^{-4}$	9.6	−13.8	−13.9	$3.995 \cdot 10^{-4}$	10.4	−13.9	−14.0
$p_{T,H} > 500$ GeV	$2.013 \cdot 10^{-3}$	37.8	−10.6	−11.6	$2.014 \cdot 10^{-3}$	37.3	−10.8	−11.7
$\lvert y_t \rvert > 2.5$	$4.961 \cdot 10^{-3}$	37.5	0.2	0.5	$5.006 \cdot 10^{-3}$	36.9	0.2	0.5

Table 5: Comparison of results from MADGRAPH5_AMC@NLO and SHERPA/MUNICH+OPENLOOPS for $pp \to t\bar{t}H$ in the setup defined in Table 1.

$pp \to W + 2j$	SHERPA/MUNICH +OPENLOOPS	ALPGEN
$H_T > 0.5$ TeV	$-8.09(2)\%$	$-4.7(2)\%$
$H_T > 1$ TeV	$-12.37(4)\%$	$-9.6(2)\%$
$H_T > 2$ TeV	$-17.8(2)\%$	$-16.6(3)\%$
$p_{T,j_1} > 0.5$ TeV	$-12.56(5)\%$	$-9.4(2)\%$
$p_{T,j_1} > 1$ TeV	$-19.1(2)\%$	$-16.0(3)\%$
$p_{T,l} > 0.5$ TeV	$-21.0(3)\%$	$-20.1(2)\%$
$p_{T,l} > 1$ TeV	$-31(1)\%$	$-31.9(5)\%$
$E_T^{miss} > 0.5$ TeV	$-22.0(3)\%$	$-20.2(2)\%$
$E_T^{miss} > 1$ TeV	$-30(1)\%$	$-31.7(4)\%$

Table 6: Relative corrections $\frac{d\sigma^{NLO}}{d\sigma^{LO}} - 1$ to the combined $W^+ + 2$ jets and $W^- + 2$ jets production processes. Comparison between the full one-loop results (SHERPA/MUNICH+OPENLOOPS) and the predictions of the logarithmic approximation (ALPGEN).

$pp \to W^- + 2j$	SHERPA/MUNICH +OPENLOOPS	ALPGEN
$H_T > 0.5$ TeV	$-8.12(2)\%$	$-4.3(2)\%$
$H_T > 1$ TeV	$-12.40(6)\%$	$-9.4(2)\%$
$H_T > 2$ TeV	$-17.7(2)\%$	$-16.6(2)\%$
$p_{T,j_1} > 0.5$ TeV	$-12.57(6)\%$	$-9.3(2)\%$
$p_{T,j_1} > 1$ TeV	$-18.9(2)\%$	$-15.3(3)\%$
$p_{T,l^-} > 0.5$ TeV	$-20.8(5)\%$	$-20.0(2)\%$
$p_{T,l^-} > 1$ TeV	$-32(2)\%$	$-32.1(3)\%$
$E_T^{miss} > 0.5$ TeV	$-21.9(4)\%$	$-20.0(3)\%$
$E_T^{miss} > 1$ TeV	$-31(1)\%$	$-32.1(3)\%$

Table 7: Relative corrections $\frac{d\sigma^{NLO}}{d\sigma^{LO}} - 1$ to $W^- + 2$ jets production. Comparison between the full one-loop results (SHERPA/MUNICH+OPENLOOPS) and the predictions of the logarithmic approximation (ALPGEN).

$pp \to W^+ + 2j$	SHERPA/MUNICH +OPENLOOPS	ALPGEN
$H_T > 0.5$ TeV	$-8.03(2)\%$	$-4.5(3)\%$
$H_T > 1$ TeV	$-12.33(6)\%$	$-9.9(2)\%$
$H_T > 2$ TeV	$-18.0(3)\%$	$-17.3(2)\%$
$p_{T,j_1} > 0.5$ TeV	$-12.56(7)\%$	$-9.5(3)\%$
$p_{T,j_1} > 1$ TeV	$-19.5(3)\%$	$-15.9(4)\%$
$p_{T,l^+} > 0.5$ TeV	$-21.1(3)\%$	$-20.1(3)\%$
$p_{T,l^+} > 1$ TeV	$-30(2)\%$	$-31.9(3)\%$
$E_T^{miss} > 0.5$ TeV	$-22.4(6)\%$	$-20.2(3)\%$
$E_T^{miss} > 1$ TeV	$-28(3)\%$	$-31.7(4)\%$

Table 8: Relative corrections $\frac{d\sigma^{NLO}}{d\sigma^{LO}} - 1$ to $W^+ + 2$ jets production. Comparison between the full one-loop results (SHERPA/MUNICH+OPENLOOPS) and the predictions of the logarithmic approximation (ALPGEN).

particle i_k. The last term in Eq. (4) comes from parameter renormalization:

$$\delta^{PR}\mathcal{M}^{NLL}_{i_1\cdots i_n} = \delta e \frac{\delta\mathcal{M}^{LO}_{i_1\cdots i_n}}{\delta e} + \delta c_w \frac{\delta\mathcal{M}^{LO}_{i_1\cdots i_n}}{\delta c_w} + \delta h_t \frac{\delta\mathcal{M}^{LO}_{i_1\cdots i_n}}{\delta h_t} + \delta h_H \frac{\delta\mathcal{M}^{LO}_{i_1\cdots i_n}}{\delta h_H}, \tag{5}$$

where $h_t = m_t/M_W$, $h_H = M_H^2/M_W^2$ and $c_w = M_W/M_Z$. In Ref. [47], the algorithm of Refs. [45, 46] has been implemented in the ALPGEN v2.1.4 [14] event generator for the vector-boson + multi-jet production and applied to study the phenomenological impact of the one-loop weak corrections to New Physics searches in missing transverse energy plus multi-jets production [47, 48, 49, 50]. Following Eq. (4), the analytic expressions of the process-independent corrections factors have been coded and all the required LO matrix elements are computed numerically by means of the ALPHA algorithm [51].

The ALPGEN results shown in Tables 6–9 have been computed by using the `vbjet` package for the production of $nW + mZ + j\gamma + lH + k$ jets with $n + m + j + l + k \leq 8$ and $k \leq 3$. In order to compare the results of the different codes, it is worth recalling the following features of the `vbjet` package: it includes only the first two generations of quarks, the external massive vector bosons are produced on-shell and the matrix elements are computed including the effect of both QCD and EW interactions. Within the `vbjet` package, the Sudakov corrections are computed using on-shell external vector bosons (the Z and W bosons are allowed to decay including spin-correlation effects only at the analyses level in order to apply the cuts listed in Table 2), they include the full logarithmic dependence in Eq. (4) for the leading $\mathcal{O}(\alpha_s^2\alpha)$ LO contributions, while they only have double logarithmic accuracy for the subleading $\mathcal{O}(\alpha^3)$ Born processes. In Refs. [45, 46] photonic contributions to virtual one-loop EW corrections are split into purely weak and purely electromagnetic terms by introducing a photon *mass* of the order of M_W: in Tables 6–9 only the weak part of the photonic contribution has been included. No real corrections have been included in the results from ALPGEN. The input parameters used for the simulation are the ones defined in Table 1, with the following exceptions for $W+2$ jets: as we are dealing with on-shell W bosons, the factorization and renormalization scale for QCD in Eq. (3) depend on M_W^2, rather than $m_{l\nu}^2$. As the NNPDF2.3 QED PDF set is not available in ALPGEN v2.1.4, we used the MSTW2008LO PDF set for both the $Z + 2$ jets and $W + 2$ jets calculations: even though this implies that a comparison at the level of cross sections is not possible for $W + 2$ jets, the PDF choice does not affect the relative corrections coming from virtual weak contributions.

In Tables 6–9 we compare the results for the full relative EW corrections, δ_{EW}^{NLO}, from Section 1.2

with the relative EW corrections calculated in the Sudakov approximation. Note that in the latter case no real corrections are included, and the virtual photonic corrections are regularized by a photon mass equal to M_{W}.

As reported in Tables 6–8 the Sudakov approximation implemented in ALPGEN and the full one-loop results are in good agreement (at the percent level) for $\mathrm{W}+2$ jets production for the distributions in the lepton transverse momentum $p_{\mathrm{T,l}}$ and the missing energy $E_{\mathrm{T}}^{\mathrm{miss}}$. For the distributions in the transverse momentum of the leading jet $p_{\mathrm{T,j_1}}$ and the variable $H_{\mathrm{T}} = p_{\mathrm{T,j_1}} + p_{\mathrm{T,j_2}} + p_{\mathrm{T,l}} + E_{\mathrm{T}}^{\mathrm{miss}}$, the Sudakov approximation tends to deviate by up to 4% from the exact fixed-order calculations in those regions of phase space where the vector boson p_{T} tends to be soft compared to the transverse momentum of the jets.

For the $\mathrm{Z}+2$ jets case shown in Table 9 this behaviour is emphasized. While the Sudakov approximation works fine for the distribution in the transverse momentum of the Z boson, deviations between the Sudakov approximation and the exact fixed-order calculation amount to 3% for the distribution in the transverse momentum of the lepton, and reach even 10% for the distributions in the transverse momentum of the leading jet $p_{\mathrm{T,j_1}}$ and the variable $H_{\mathrm{T}} = p_{\mathrm{T,j_1}} + p_{\mathrm{T,j_2}} + p_{\mathrm{T,l^+}} + p_{\mathrm{T,l^-}}$. It is worth noticing, however, that for $\mathrm{Z}+2$ jets the difference between the ALPGEN predictions and the full one-loop results also originates from the on-shell approximation, as in this approximation the contribution of the diagrams containing a photon connecting the lepton pair to a quark line in the process $\mathrm{pp} \to \mathrm{l^+l^-} + 2$ jets is not included.

1.4 Ratio of the Z to gamma transverse momentum differential cross-section

The ratio of the associated production of a Z/γ^* or a γ with one or more jets has been recently measured in proton–proton collisions at 8 TeV center-of-mass energy by the CMS Collaboration at the CERN LHC [52]. In the limit of high transverse momentum of the vector boson p_{T}^V ($V = \mathrm{Z}, \gamma$) and at LO in perturbative quantum chromodynamics (QCD), effects due to the mass of the Z boson (M_{Z}) are small, and the cross section ratio of Z + jets to γ + jets as a function of p_{T}^V is expected to become constant, reaching a plateau for $p_{\mathrm{T}}^V \geq 300$ GeV [53]. (Hereafter, production of Z/γ^* + jets is denoted by Z + jets.) A QCD calculation at NLO for pp$\to$ Z + jets and pp$\to$ γ + jets was provided by the BLACKHAT Collaboration [54]. The NLO QCD corrections tend to decrease the value of the cross section ratio. At higher energies, EW corrections can also introduce a dependence of the cross section on logarithmic terms of the form $\ln(p_{\mathrm{T}}^{\mathrm{Z}}/m_{\mathrm{Z}})$ that become large and pose a challenge for perturbative calculations.

Searches for new particles involving final states characterized by the presence of large missing transverse energy and hard jets, use the γ + jets process to model the invisible Z decays, $\mathrm{Z}\to \nu\bar{\nu}$, since the γ + jets cross section is larger than the Z + jets process where the Z decays to leptons. A precise estimate of EW corrections on the cross section ratio for Z + jets and γ + jets is therefore crucial to reduce uncertainties related to the $\mathrm{Z}\to \nu\bar{\nu}$ background estimation in these searches.

In the CMS measurement [52], results are unfolded into a fiducial region defined at particle level. For Z + jets events, the leading leptons are required to have $p_{\mathrm{T}} > 20$ GeV and $|\eta| < 2.4$, while jets are required to have $p_{\mathrm{T}} > 30$ GeV within the region of $|\eta| < 2.4$. Electrons and muons have different energy losses due to final-state radiation at particle level. In order to compensate for these differences, a "dressed" level is defined to make the electron and muon channels compatible to within 1%. This is achieved by defining in simulation a particle momentum vector by adding the momentum of the stable lepton and the momenta of all photons with a radius of $\Delta R = 0.1$ around the stable lepton. All jets are required to be separated from each lepton by $\Delta R > 0.5$. At the particle level, a true isolated photon is defined as a prompt photon, around which the scalar sum of the p_{T} of all stable particles in a cone of radius $\Delta R = 0.4$ is less than 5 GeV. A true isolated photon is defined as a prompt photon (not generated by a hadron decay), around which the scalar sum of the p_{T} of all stable particles in a cone of radius $\Delta R = 0.4$ is less than 5 GeV. When comparing the cross sections for Z + jets and γ + jets, the rapidity range of the bosons is restricted to $|y^V| < 1.4$ because this is the selected kinematic region for

$pp \to Z + 2j$	RECOLA full	RECOLA*	ALPGEN
inclusive	$-2.47(2)\%$	$-2.69(2)\%$	–
$H_T > 0.5$ TeV	$-7.05(3)\%$	$-7.38(3)\%$	$-5.2(3)\%$
$H_T > 1$ TeV	$-12.79(4)\%$	$-13.41(5)\%$	$-10.4(1)\%$
$H_T > 1.5$ TeV	$-17.59(8)\%$	$-18.70(9)\%$	$-13.7(1)\%$
$H_T > 2$ TeV	$-21.7(2)\%$	$-23.8(2)\%$	$-14.9(2)\%$
$m_{jj} > 0.5$ TeV	$-4.33(5)\%$	$-4.56(5)\%$	$-1.4(3)\%$
$m_{jj} > 1$ TeV	$-5.76(8)\%$	$-6.03(8)\%$	$-2(1)\%$
$m_{jj} > 2$ TeV	$-7.3(1)\%$	$-7.6(1)\%$	$-6(1)\%$
$m_{jj} > 4$ TeV	$-8.2(2)\%$	$-8.5(2)\%$	$-15(2)\%$
$p_{T,j_1} > 0.25$ TeV	$-7.64(3)\%$	$-7.99(3)\%$	$-5.8(1)\%$
$p_{T,j_1} > 0.5$ TeV	$-13.09(6)\%$	$-13.83(6)\%$	$-10.4(1)\%$
$p_{T,j_1} > 0.75$ TeV	$-17.5(1)\%$	$-19.0(1)\%$	$-13.0(1)\%$
$p_{T,j_1} > 1$ TeV	$-21.4(2)\%$	$-24.1(3)\%$	$-14.0(2)\%$
$p_{T,l^-} > 0.25$ TeV	$-12.93(8)\%$	$-13.47(9)\%$	$-11.0(1)\%$
$p_{T,l^-} > 0.5$ TeV	$-20.5(2)\%$	$-21.1(2)\%$	$-18.7(1)\%$
$p_{T,l^-} > 0.75$ TeV	$-26.3(4)\%$	$-26.9(4)\%$	$-23.9(1)\%$
$p_{T,l^-} > 1$ TeV	$-30.9(8)\%$	$-31.3(9)\%$	$-28.4(2)\%$
$p_{T,Z} > 0.25$ TeV	$-9.31(4)\%$	$-9.77(4)\%$	$-8.5(1)\%$
$p_{T,Z} > 0.5$ TeV	$-16.37(8)\%$	$-16.9(8)\%$	$-16.3(1)\%$
$p_{T,Z} > 0.75$ TeV	$-22.0(1)\%$	$-22.5(1)\%$	$-21.7(1)\%$
$p_{T,Z} > 1$ TeV	$-27.1(4)\%$	$-27.6(4)\%$	$-26.8(2)\%$

Table 9: Relative corrections $\frac{d\sigma^{NLO}}{d\sigma^{LO}} - 1$ to $Z + 2$ jets production. Comparison between the full one-loop results (RECOLA) and the predictions of the logarithmic approximation (ALPGEN, SHERPA). RECOLA* is the full one-loop result where the contribution of b-quarks has been removed from both LO and NLO and the contribution of gluon radiation has been removed from the NLO.

the photons. The ratio of the differential cross sections as a function of p_{T} is measured in the phase-space regions: $N_{\mathrm{jets}} \geq 1$, 2, 3 and $H_{\mathrm{T}} > 300$ GeV, $N_{\mathrm{jets}} \geq 1$.

Figure 1 compares several predictions for the ratio within the fiducial regions as defined above[5]. The fixed-order partonic predictions computed with the ALPGEN generator are shown at LO and at approximated NLO accuracy [47], i.e. including the effect of virtual weak corrections in the Sudakov approximation obtained by means of the algorithm of Refs. [45, 46], as described in Section 1.3. The predictions for Z + jets and γ + jets are computed in the G_μ and $\alpha(0)$ schemes, respectively, with the set of parameters listed above for the calculation of the $\mathcal{O}(\alpha)$ corrections to the process $\mathrm{W} + 2$ jets. The factorization scale is set to $\sum_j p_{\mathrm{T}}^j + \sqrt{M_V^2 + p_{\mathrm{T},V}^2}$. CTEQ5L is used as PDF set: it is worth noticing, however, that PDFs largely cancel in the Z/γ ratio as pointed out in Ref. [55]. More precisely, the predictions for γ + jets and Z + jets are computed by using the phjet and zjet packages, respectively: at variance with the vbjet package, where the external vector bosons are produced on-shell, in zjet the Z boson decays in a fermion–antifermion pair including all the off-shell and spin-correlation effects. These packages include only the QCD contributions of order $\alpha_s^{n\,\mathrm{jets}}\alpha$ to the LO predictions. Though the LO results for Z + jets include exactly off-shell and spin-correlation effects, the Sudakov corrections are obtained in the on-shell approximation by using the phase-space mapping described in Ref. [23].

The other predictions are also shown in the CMS paper, where a detailed description of the configuration used can be found. For Z + jets and γ + jets generated with the MADGRAPH5 [56] program, the LO multiparton matrix-element calculation includes up to four partons in the final state. The showering and hadronization, as well as the underlying event, are modelled by PYTHIA6 [57]. The events are generated with the CTEQ6L1 [58] parton distribution functions, and the ktMLM matching scheme [59] with a matching parameter of 20 GeV is applied. In addition to these Monte Carlo signal data sets, a NLO perturbative QCD calculation from the BLACKHAT Collaboration [54] is available for a boson accompanied by up to three jets. These calculations use MSTW2008nlo68cl [60] with $\alpha_s = 0.119$ as the PDF set, and the renormalization and factorization scales are set to $\mu_{\mathrm{R}} = \mu_{\mathrm{F}} = H_{\mathrm{T}} + E_{\mathrm{T}}^{\mathrm{V}}$, where H_{T} is the scalar p_{T} sum of all outgoing partons with $p_{\mathrm{T}} > 20$ GeV and $E_{\mathrm{T}}^{\mathrm{V}}$ is defined as $\sqrt{m_{\mathrm{Z}}^2 + \left(p_{\mathrm{T}}^{\mathrm{Z}}\right)^2}$ and p_{T}^{γ}, respectively, for Z + jets and γ + jets. In addition, the photons must satisfy the Frixione cone isolation condition [61].

From the plot it is clear that both NLO QCD and EW corrections are negative with respect to the fixed-order LO predictions. The NLO QCD corrections are larger for lower transverse momentum of the bosons, reaching a 15% effect for $N_{\mathrm{jets}} \geq 1$. A fraction of this effect seems to be included by MADGRAPH5 predictions, which include higher-order real-parton emissions in the matrix-element calculation. The EW corrections increase with the boson transverse momentum, up to about 10% for $p_{\mathrm{T}} > 600$ GeV in events with at least one jet. Both QCD and EW corrections decrease for larger jet multiplicities. It can be also noticed that the Madgraph prediction overshoots the NLO QCD ones for larger multiplicities.

In Figure 2, these predictions are compared to CMS results, showing that the agreement improves when NLO corrections are included, both in the case of QCD and EW ones. In particular, including the EW corrections, results are in better agreement in the region of high boson transverse-momenta, especially for larger jet multiplicities.

Finally, Figure 3 shows in addition, for events with a vector boson and at least one jet, fixed-order predictions from Sherpa+OpenLoops. The Z + jets prediction is obtained from an off-shell calculation for $\mathrm{l}^+\mathrm{l}^-$ + jets including all Z/γ^* interference effects. The presented predictions are based on the recently achieved automation of NLO QCD+EW calculations [11, 26], as described in Section 1.2. Related predictions for the Z+jets/γ+jets ratio (with an on-shell Z boson) from Munich+OpenLoops have already been presented in Ref. [62] and have for example been employed for background predic-

[5] We dropped the comparison for $H_{\mathrm{T}} > 300$ GeV because fixed-order predictions are known to fail describing high jet activity with a comparatively low vector boson p_{T}.

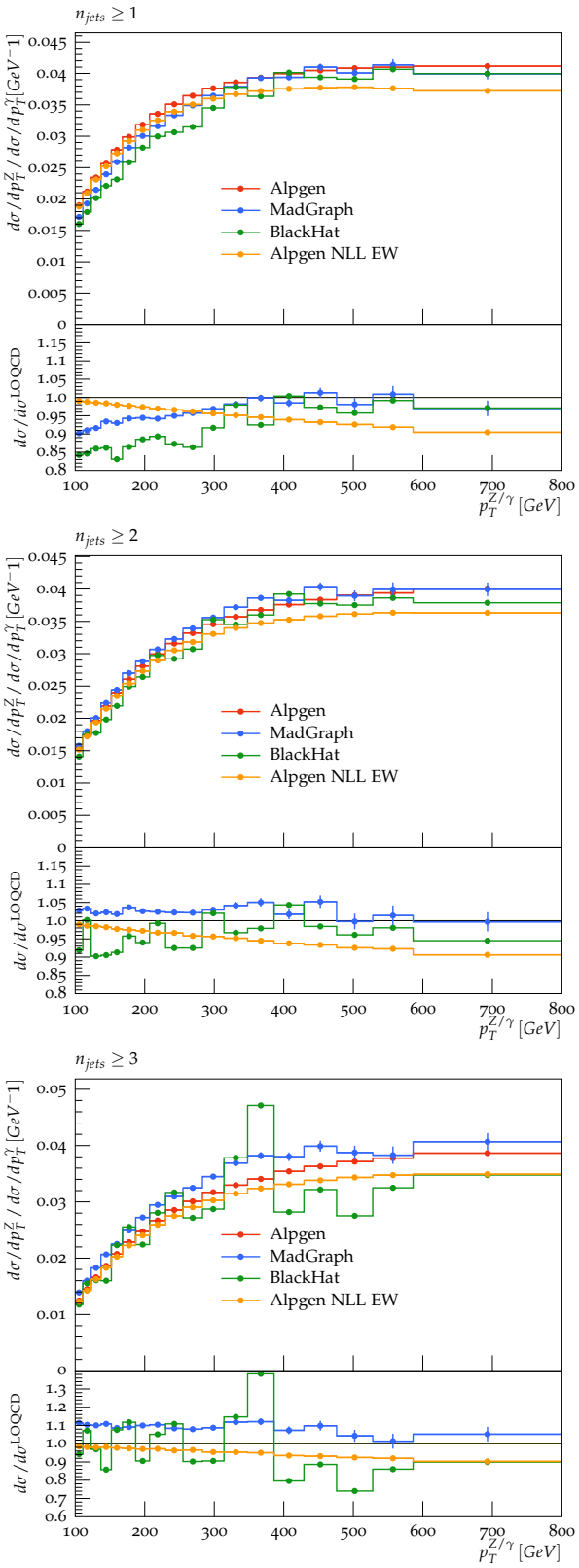

Fig. 1: Comparison of different predictions for the ratio of Z + jets over γ + jets at 8 TeV pp center-of-mass energy. From top to bottom, results are shown for events with at least 1, 2 and 3 jets accompanying the boson. For fixed-order predictions this value corresponds to the number of partons in the final state at the lowest order.

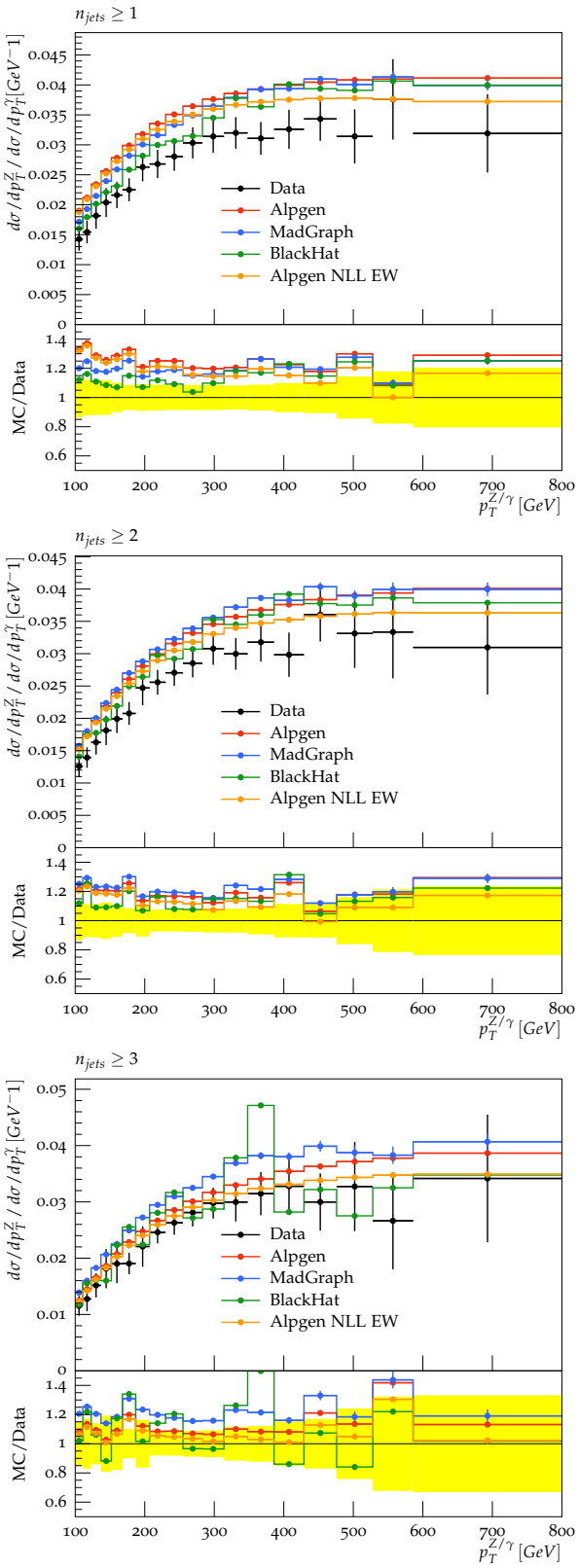

Fig. 2: Comparison to CMS data of different predictions for the ratio of Z + jets over γ + jets at 8 TeV pp center-of-mass energy. From top to bottom, results are shown for events with at least 1, 2 and 3 jets accompanying the boson. For fixed-order predictions this value corresponds to the number of partons in the final state at the lowest order.

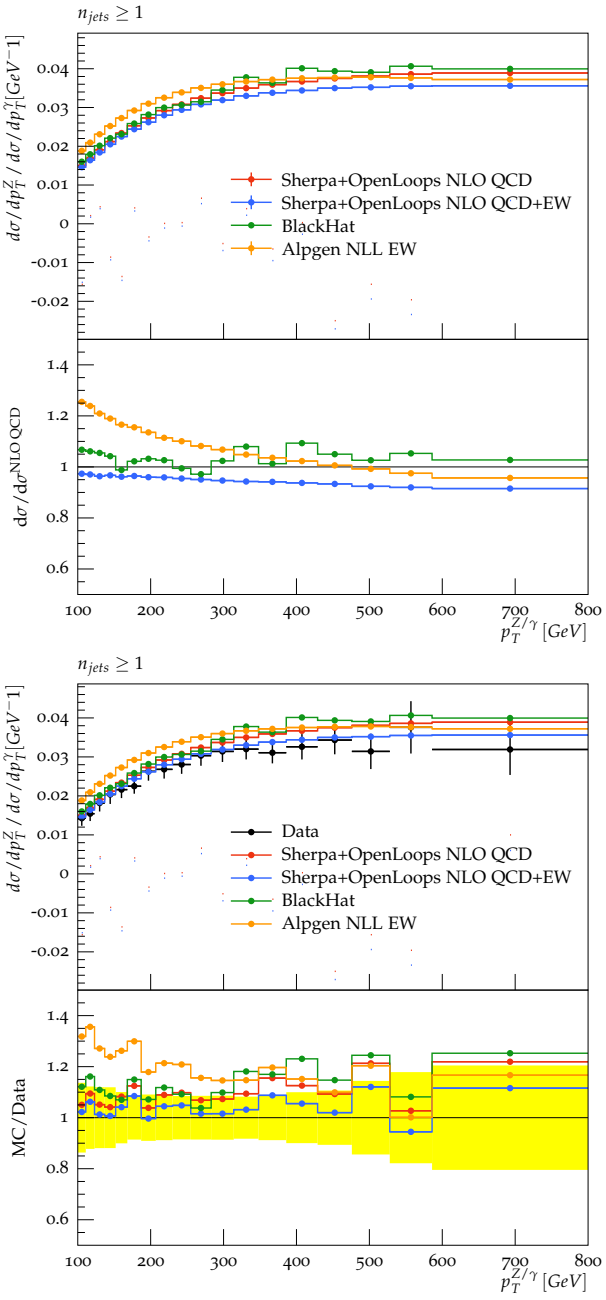

Fig. 3: Comparison of different predictions at NLO QCD, NLL EW and NLO QCD+EW order for the ratio of Z + jets over γ + jets at 8 TeV pp center-of-mass energy, in events with at least 1 jet accompanying the boson. For fixed-order predictions this value corresponds to the number of partons in the final state at the lowest order. The top plot shows a comparison among the predictions, the bottom plot a comparison to CMS data.

tions in Ref. [63]. Here, we employ NNPDF2.3QED [64] parton distributions with $\alpha_s = 0.118$, and all input parameters and scale choices are as detailed in Ref. [26]. In particular, all unstable particles are treated in the complex-mass scheme [20], and renormalization and factorization scales are set to $\mu_{\mathrm{R,F}} = \hat{H}'_{\mathrm{T}}/2$, where $\hat{H}'_{\mathrm{T}}$ is the scalar sum of the transverse energy of all parton-level final-state objects, $\hat{H}'_{\mathrm{T}} = \sum_{i\in\{\mathrm{quarks,gluons}\}} p_{\mathrm{T},i} + p_{\mathrm{T},\gamma} + E_{\mathrm{T},V}$. QCD partons and photons that are radiated at NLO are included in $\hat{H}'_{\mathrm{T}}$, and the vector-boson transverse energy, $E_{\mathrm{T},V}$, is computed using the total (off-shell) four-momentum of the corresponding (dressed) decay products, i.e. $E^2_{\mathrm{T,Z}} = p^2_{\mathrm{T,ll}} + m^2_{\mathrm{ll}}$ and $E^2_{\mathrm{T},\gamma} = p^2_{\mathrm{T},\gamma}$. The weak coupling constant α is renormalized in the G_μ scheme for the $\mathrm{l}^+\mathrm{l}^-$ + jets prediction, while the $\alpha(0)$ scheme is used for the γ + jets prediction. Results are presented at the NLO QCD level and combining QCD and EW corrections via an additive prescription, i.e. $\sigma^{\mathrm{NLO}}_{\mathrm{QCD+EW}} = \sigma^{\mathrm{LO}} + \delta\sigma^{\mathrm{NLO}}_{\mathrm{QCD}} + \delta\sigma^{\mathrm{NLO}}_{\mathrm{EW}}$. Isolated photons in the γ + jets predictions are required to satisfy Frixione cone isolation [61] with parameters as specified in Ref. [52].

The agreement of the combined NLO QCD+EW prediction with the CMS data is remarkable over the whole spectrum. As already noted, at low transverse momentum NLO QCD corrections to the ratio are relevant due to mass effects, but sizable EW corrections due to EW Sudakov logarithms (of different size for the two processes) alter the shape of the ratio prediction already much below 1 TeV. These results show the importance of combining NLO QCD and EW corrections in a unified framework.

1.5 Conclusions

In this contribution we have performed a comparison of calculations of EW corrections between different automated codes. While it is a non-trivial task to precisely adjust the settings of the different calculations such that they are consistent with each other, we found a typical agreement at the level of one per cent. We also compared the Sudakov approximation to exact NLO calculations. Depending on the considered process and the considered observable the Sudakov approximation can describe the complete EW NLO corrections at the level of one to ten per cent. When comparing CMS data for the ratio of the associated production of a Z/γ^* or an on-shell photon with one or more jets to theoretical predictions, the inclusion of EW corrections results in a better agreement for high boson transverse momenta.

Acknowledgements

The work of A. Denner was supported by the Deutsche Forschungsgemeinschaft (DFG) under reference number DE 623/2-1. The work of D. Pagani is supported by the ERC grant 291377 "LHCtheory: Theoretical predictions and analyses of LHC physics: advancing the precision frontier". M. Zaro is supported by the European Union's Horizon 2020 research and innovation programme under the Marie Sklodovska-Curie grant agreement No 660171 and in part by the ILP LABEX (ANR-10-LABX-63), in turn supported by French state funds managed by the ANR within the "Investissements d'Avenir" programme under reference ANR-11-IDEX-0004-02.

References

[1] T. Hahn and M. Perez-Victoria, *Comput.Phys.Commun.* **118** (1999) 153–165, [hep-ph/9807565].

[2] K. Arnold *et. al.*, *Comput. Phys. Commun.* **180** (2009) 1661–1670, [0811.4559].

[3] C. Berger, Z. Bern, L. Dixon, F. Febres Cordero, D. Forde, *et. al.*, *Phys.Rev.* **D78** (2008) 036003, [0803.4180].

[4] S. Becker, C. Reuschle, and S. Weinzierl, *JHEP* **12** (2010) 013, [1010.4187].

[5] S. Badger, B. Biedermann, and P. Uwer, *Comput.Phys.Commun.* **182** (2011) 1674–1692, [1011.2900].

[6] V. Hirschi, R. Frederix, S. Frixione, M. V. Garzelli, F. Maltoni, *et. al.*, *JHEP* **1105** (2011) 044, [1103.0621].

[7] G. Bevilacqua, M. Czakon, M. Garzelli, A. van Hameren, A. Kardos, *et. al.*, *Comput.Phys.Commun.* **184** (2013) 986–997, [1110.1499].

[8] G. Cullen, N. Greiner, G. Heinrich, G. Luisoni, P. Mastrolia, *et. al.*, *Eur.Phys.J.* **C72** (2012) 1889, [1111.2034].

[9] F. Cascioli, P. Maierhöfer, and S. Pozzorini, *Phys.Rev.Lett.* **108** (2012) 111601, [1111.5206].

[10] S. Actis, A. Denner, L. Hofer, A. Scharf, and S. Uccirati, *JHEP* **1304** (2013) 037, [1211.6316].

[11] S. Kallweit, J. M. Lindert, P. Maierhöfer, S. Pozzorini, and M. Schönherr, *JHEP* **04** (2015) 012, [1412.5157].

[12] S. Frixione, V. Hirschi, D. Pagani, H. S. Shao, and M. Zaro, *JHEP* **09** (2014) 065, [1407.0823].

[13] M. Chiesa, N. Greiner, and F. Tramontano, *J. Phys.* **G43** (2016), no. 1 013002, [1507.08579].

[14] M. L. Mangano, M. Moretti, F. Piccinini, R. Pittau, and A. D. Polosa, *JHEP* **0307** (2003) 001, [hep-ph/0206293].

[15] A. van Hameren, *JHEP* **0907** (2009) 088, [0905.1005].

[16] A. Denner, *Fortsch.Phys.* **41** (1993) 307–420, [0709.1075].

[17] M. V. Garzelli, I. Malamos, and R. Pittau, *JHEP* **01** (2010) 040, [0910.3130]. [Erratum: JHEP10,097(2010)].

[18] A. Denner, S. Dittmaier, and L. Hofer, *PoS* **LL2014** (2014) 071, [1407.0087].

[19] A. Denner, S. Dittmaier, and L. Hofer,, "COLLIER: a complex one-loop library with extended regularizations." http://collier.hepforge.org, 2016.

[20] A. Denner, S. Dittmaier, M. Roth, and L. Wieders, *Nucl.Phys.* **B724** (2005) 247–294, [hep-ph/0505042]. Erratum-ibid. **B854** (2012) 504–507.

[21] S. Catani and M. H. Seymour, *Nucl. Phys.* **B485** (1997) 291–419, [hep-ph/9605323].

[22] S. Catani, S. Dittmaier, M. H. Seymour, and Z. Trocsanyi, *Nucl. Phys.* **B627** (2002) 189–265, [hep-ph/0201036].

[23] A. Denner, L. Hofer, A. Scharf, and S. Uccirati, *JHEP* **01** (2015) 094, [1411.0916].

[24] A. Denner and R. Feger, 1506.07448.

[25] F. Cascioli, J. Lindert, P. Maierhöfer, and S. Pozzorini,, "OPENLOOPS one-loop generator." http://openloops.hepforge.org, 2012.

[26] S. Kallweit, J. M. Lindert, S. Pozzorini, M. Schönherr, and P. Maierhöfer, 1511.08692.

[27] A. Denner and S. Dittmaier, *Nucl. Phys.* **B658** (2003) 175–202, [hep-ph/0212259].

[28] A. Denner and S. Dittmaier, *Nucl. Phys.* **B734** (2006) 62–115, [hep-ph/0509141].

[29] A. Denner and S. Dittmaier, *Nucl.Phys.* **B844** (2011) 199–242, [1005.2076].

[30] G. Ossola, C. G. Papadopoulos, and R. Pittau, *JHEP* **0803** (2008) 042, [0711.3596].

[31] G. Ossola, C. G. Papadopoulos, and R. Pittau, *Nucl. Phys.* **B763** (2007) 147–169, [hep-ph/0609007].

[32] A. van Hameren, *Comput.Phys.Commun.* **182** (2011) 2427–2438, [1007.4716].

[33] MUNICH is the abbreviation of "MUlti-chaNnel Integrator at Swiss (CH) precision"—an automated parton level NLO generator by S. Kallweit, in preparation.

[34] T. Gleisberg and F. Krauss, *Eur. Phys. J.* **C53** (2008) 501–523, [0709.2881].

[35] T. Gleisberg, S. Höche, F. Krauss, M. Schonherr, S. Schumann, *et. al.*, *JHEP* **0902** (2009) 007, [0811.4622].

[36] F. Krauss, R. Kuhn, and G. Soff, *JHEP* **02** (2002) 044, [hep-ph/0109036].

[37] T. Gleisberg and S. Hoeche, *JHEP* **12** (2008) 039, [0808.3674].

[38] S. Dittmaier, *Nucl. Phys.* **B565** (2000) 69–122, [hep-ph/9904440].

[39] S. Dittmaier, A. Kabelschacht, and T. Kasprzik, *Nucl. Phys.* **B800** (2008) 146–189, [0802.1405].

[40] J. Alwall, R. Frederix, S. Frixione, V. Hirschi, F. Maltoni, O. Mattelaer, H. S. Shao, T. Stelzer, P. Torrielli, and M. Zaro, *JHEP* **07** (2014) 079, [1405.0301].

[41] S. Frixione, V. Hirschi, D. Pagani, H. S. Shao, and M. Zaro, *JHEP* **06** (2015) 184, [1504.03446].

[42] R. Frederix, S. Frixione, F. Maltoni, and T. Stelzer, *JHEP* **10** (2009) 003, [0908.4272].

[43] C. Degrande, C. Duhr, B. Fuks, D. Grellscheid, O. Mattelaer, and T. Reiter, *Comput. Phys. Commun.* **183** (2012) 1201–1214, [1108.2040].

[44] M. Cacciari, M. Greco, and P. Nason, *JHEP* **05** (1998) 007, [hep-ph/9803400].

[45] A. Denner and S. Pozzorini, *Eur.Phys.J.* **C18** (2001) 461–480, [hep-ph/0010201].

[46] A. Denner and S. Pozzorini, *Eur.Phys.J.* **C21** (2001) 63–79, [hep-ph/0104127].

[47] M. Chiesa, G. Montagna, L. Barze, M. Moretti, O. Nicrosini, *et. al.*, *Phys.Rev.Lett.* **111** (2013), no. 12 121801, [1305.6837].

[48] K. Mishra, T. Becher, L. Barze, M. Chiesa, S. Dittmaier, *et. al.*, 1308.1430.

[49] J. Campbell, K. Hatakeyama, J. Huston, F. Petriello, J. R. Andersen, *et. al.*, 1310.5189.

[50] J. Butterworth, G. Dissertori, S. Dittmaier, D. de Florian, N. Glover, *et. al.*, 1405.1067.

[51] F. Caravaglios and M. Moretti, *Phys.Lett.* **B358** (1995) 332–338, [hep-ph/9507237].

[52] V. Khachatryan *et. al.*,, **CMS** Collaboration *JHEP* **10** (2015) 128, [1505.06520].

[53] S. Ask, M. A. Parker, T. Sandoval, M. E. Shea, and W. J. Stirling, *J. High Energy Phys.* **10** (2011) 058, [1107.2803].

[54] Z. Bern, G. Diana, L. J. Dixon, F. Febres Cordero, S. Höche, H. Ita, D. A. Kosower, D. Maître, and K. J. Ozeren, *Phys. Rev. D* **87** (2013) 034026, [1206.6064].

[55] S. Ask, M. A. Parker, T. Sandoval, M. E. Shea, and W. J. Stirling, *JHEP* **10** (2011) 058, [1107.2803].

[56] J. Alwall, M. Herquet, F. Maltoni, O. Mattelaer, and T. Stelzer, *J. High Energy Phys.* **06** (2011) 128, [1106.0522].

[57] T. Sjöstrand, S. Mrenna, and P. Skands, *J. High Energy Phys.* **05** (2006) 026, [hep-ph/0603175].

[58] J. Pumplin, D. R. Stump, J. Huston, H.-L. Lai, P. Nadolsky, and W.-K. Tung, *J. High Energy Phys.* **07** (2002) 012, [hep-ph/0201195].

[59] J. Alwall, S. Höche, F. Krauss, N. Lavesson, L. Lönnblad, F. Maltoni, M. L. Mangano, M. Moretti, C. G. Papadopoulos, F. Piccinini, S. Schumann, M. Treccani, J. Winter, and M. Worek, *Eur. Phys. J. C* **53** (2008) 473, [0706.2569].

[60] A. D. Martin, W. J. Stirling, R. S. Thorne, and G. Watt, *Eur. Phys. J. C* **63** (2009) 189, [0901.0002].

[61] S. Frixione, *Phys. Lett. B* **429** (1998) 369, [hep-ph/9801442].

[62] S. Kallweit, J. M. Lindert, S. Pozzorini, M. Schnherr, and P. Maierhfer, in *Proceedings, 50th Rencontres de Moriond, QCD and high energy interactions*, pp. 121–124, 2015. 1505.05704.

[63] CMS Collaboration,, "Search for dark matter with jets and missing transverse energy at 13 TeV." CMS-PAS-EXO-15-003, 2015.

[64] R. D. Ball, V. Bertone, S. Carrazza, L. Del Debbio, S. Forte, A. Guffanti, N. P. Hartland, and J. Rojo,, **NNPDF** Collaboration *Nucl. Phys.* **B877** (2013) 290–320, [1308.0598].